

# High Contrast Imaging with METIS

Matthew A. Kenworthy<sup>a</sup>, Olivier Absil<sup>b</sup>, Tibor Agocs<sup>c</sup>, Eric Pantin<sup>d</sup>, Sascha P. Quanz<sup>e</sup>,  
Remko Stuik<sup>a</sup>, Frans Snik<sup>a</sup>, and Bernhard R. Brandl<sup>a</sup>

<sup>a</sup>Leiden Observatory, Leiden University, P.O. Box 9513, 2300 RA Leiden, The Netherlands

<sup>b</sup>Space sciences, Technologies, and Astrophysics Research (STAR) Institute, University of  
Liège, 19c allée du Six Août, B-4000 Sart Tilman, Belgium

<sup>c</sup>NOVA-ASTRON, P.O. Box 2, 7990 AA Dwingeloo, The Netherlands

<sup>d</sup>Groupe LFEPS, Service d'Astrophysique, CE Saclay DSM/DAPNIA/Sap, 91191 Gif sur  
Yvette Cedex, France

<sup>e</sup>ETH Zürich; Institute for Astronomy, Wolfgang-Pauli-Strasse 27, CH-8093 Zürich,  
Switzerland

## ABSTRACT

The Mid-infrared E-ELT Imager and Spectrograph (METIS) for the European Extremely Large Telescope (E-ELT) consists of diffraction-limited imagers that cover 3 to 14 microns with medium resolution ( $R \sim 5000$ ) long slit spectroscopy, and an integral field spectrograph for high spectral resolution spectroscopy ( $R \sim 100,000$ ) over the L and M bands. One of the science cases that METIS addresses is the characterization of faint circumstellar material and exoplanet companions through imaging and spectroscopy.

We present our approach for high contrast imaging with METIS, covering diffraction suppression with coronagraphs, the removal of slowly changing optical aberrations with focal plane wavefront sensing, interferometric imaging with sparse aperture masks, and observing strategies for both the imagers and IFU image slicers.

**Keywords:** E-ELT, high contrast imaging, coronagraphs, thermal IR

## 1. INTRODUCTION

The METIS High Contrast Imaging (HCI) work package covers all aspects of imaging in the speckle-dominated domain, where the sky background limit is not reachable due to the diffraction halo of a bright unresolved source. The most typical science case is that of imaging faint point and extended structures around stars, including extrasolar planets and debris disks. There are HCI observing modes for both imaging and spectroscopy. METIS has two imaging cameras, a long slit spectroscopy mode that uses grisms in the imagers, and one high L and M spectral resolution integral field mode.

## 2. HIGH CONTRAST IMAGING

The HCI modes have small inner working angles (IWAs) to exploit the large diameter of the E-ELT, and are implemented using three different sets of optics - focal plane coronagraphs, pupil plane coronagraphs, and interferometric imaging masks. Focal plane coronagraphs include variations based on the vortex coronagraph (VC), pupil plane coronagraphs based on the vector Apodizing Phase Plate (vAPP), and a goal of high spatial resolution interferometry with Sparse Aperture Masking (SAM) techniques.

The VC are high throughput coronagraphs that provide 360 degrees of diffraction suppression around the central star down to an IWA of  $\sim 1.1\lambda/D$ , but their nulling depth is sensitive to residual vibrations from the telescope and atmosphere that cannot be removed by the AO system, and by atmospheric dispersion at large zenith distances. METIS does not have an atmospheric dispersion corrector for the science path, and it is not expected to have one installed.

---

E-mail: kenworthy@strw.leidenuniv.nl, Telephone: +31 (0)71 527 8455

The vAPP coronagraph provides robust performance with lower throughput than the best VC designs and is insensitive to telescope vibrations, and provide beam switching at thermal infrared wavelengths. Their IWA reaches down to  $\sim 2\lambda/D$ .

SAM is a single dish interferometric technique that masks out the majority of the telescope pupil to make a set of apertures with non-redundant pairs of baselines. Visibilities of the resultant fringes in the science camera focal plane can then be used to reconstruct the image of the source and reaches angular resolutions of  $0.5\lambda/D$ , but have significantly lower throughput than the other HCI modes.

### 3. OPTICAL PATH OF LIGHT IN METIS

A schematic overview of the light path in METIS along with the relevant pupil and focal plane locations for the HCI components is shown in Figure 1. Light comes in and reflects off of the primary mirror M1, which is formed from 798 of close-packed hexagonal elements, each 1.45m from side to side.<sup>1</sup> A certain number of these mirrors may have low reflectivity or are removed for cleaning and recoating, the number is expected to be between 3 and 7 on any given night of observing. The telescope pupil is then reimaged through two more mirrors onto M4, which is an adaptively controlled mirror that provides adaptive optics correction for distortions introduced by atmospheric turbulence. Light forms the final telescope focal plane in front of METIS, and passes into the cryogenically cooled Common Fore Optics (CFO) of the instrument.<sup>2</sup>

The E-ELT focal plane is formed in front of the entrance window of METIS. The focal plane is reimaged twice in the CFO which is shown in Figure 2. The first image relay provides a transmissive pupil plane for the cold stop PP1, which is undersized with respect to M1 and M4 and defines the stop for the METIS instrument. The cold stop mask rotates with the telescope pupil to ensure that the warm secondary support structure and central obscuration do not contribute to the thermal background in METIS. Located close to PP1 is an additional mechanism to move masks in and out of the pupil plane. This mechanism will not have a rotation mechanism for pupil tracking. The light then passes through a K-mirror that can rotate the optical beam with an angular speed that either tracks the sky rotation or keeps the cold stop pupil image fixed with respect to the other pupil and focal planes in METIS. The focal plane FP1 is formed just after the derotator, and then the AO pickoff dichroic reflects short wavelength light into the SCAO wavefront sensor and passes the longer wavelength light through to METIS. A second relay based on an all reflective Offner design forms a spherical surface pupil image PP2 for the chopper mirror (this location inaccessible for additional optics) and forms the second focal plane FP2. FP2 contains a wheel mechanism that contains the Annular Groove Phase Masks that are part of the Vortex Coronagraph, and long slits that form the entrance to the spectroscopic modes of the imaging cameras.

For imaging, there are two separate cameras, one for L and M bands, and a separate one for N band. Both cameras have a pupil plane, PP3, that can contain apodizers and masks for HCI. In this paper, we schematically combine these into one imaging camera and refer to them as the IMG mode.

A movable pick-off mirror can be inserted into the science beam beyond FP2, sending light into the high spectral resolution LM Spectrograph (LMS). The LMS has a separate pupil wheel in front of the image slicer, where HCI optics can be located.

Together, PP1, FP1, FP2, and PP3 provide a wide range of combinations for the different HCI modes. It should be noted that PP1 and FP1 are both above the AO dichroic, and any optics placed in these beams are visible to the WFS camera. PP1 is also above the derotator, and so any optic there will have the telescope pupil rotate during an observation.

### 4. CORONAGRAPHIC CONFIGURATIONS

Simulations of coronagraphs in METIS<sup>3</sup> show that two coronagraphic configurations should be considered as baseline - the vAPP coronagraphs and the Vortex Coronagraph-Lyot Phase Mask (VC-LPM) coronagraphs. The contrast curves that show the performance of the different coronagraphs are shown in Figure 3.

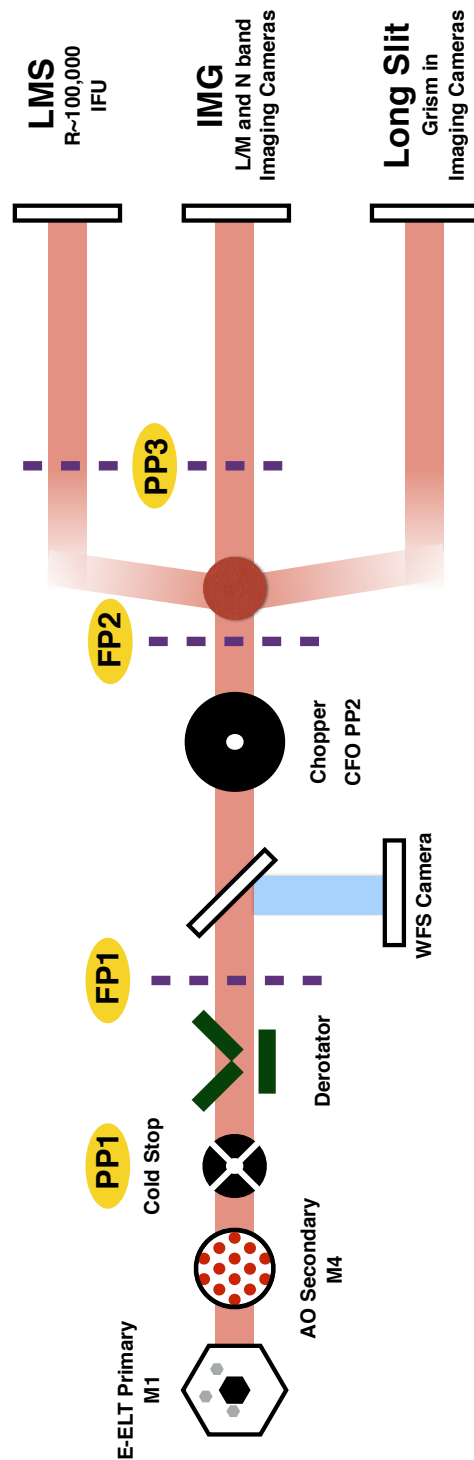


Figure 1. Schematic layout of the relevant optical components for HCI in METIS. The imaging cameras are represented as two separate paths labelled “IMG - Imaging Camera” and “Long Slit - Grism in IMG” to emphasise the different possible optical configurations. The accessible focal plane and pupil planes are labelled in a yellow ellipse.

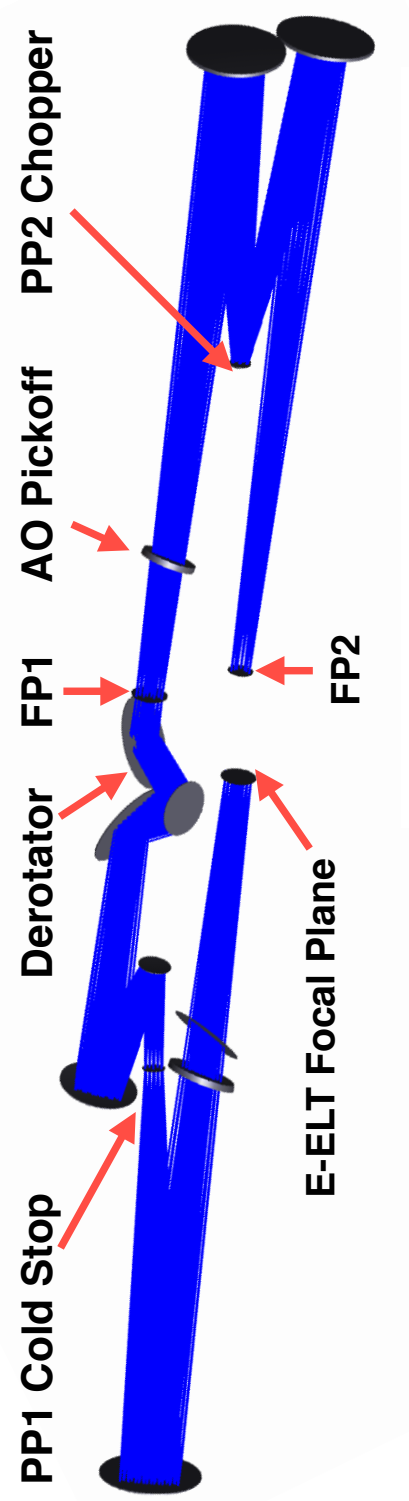


Figure 2. Optical layout of the Common Fore Optics for METIS.

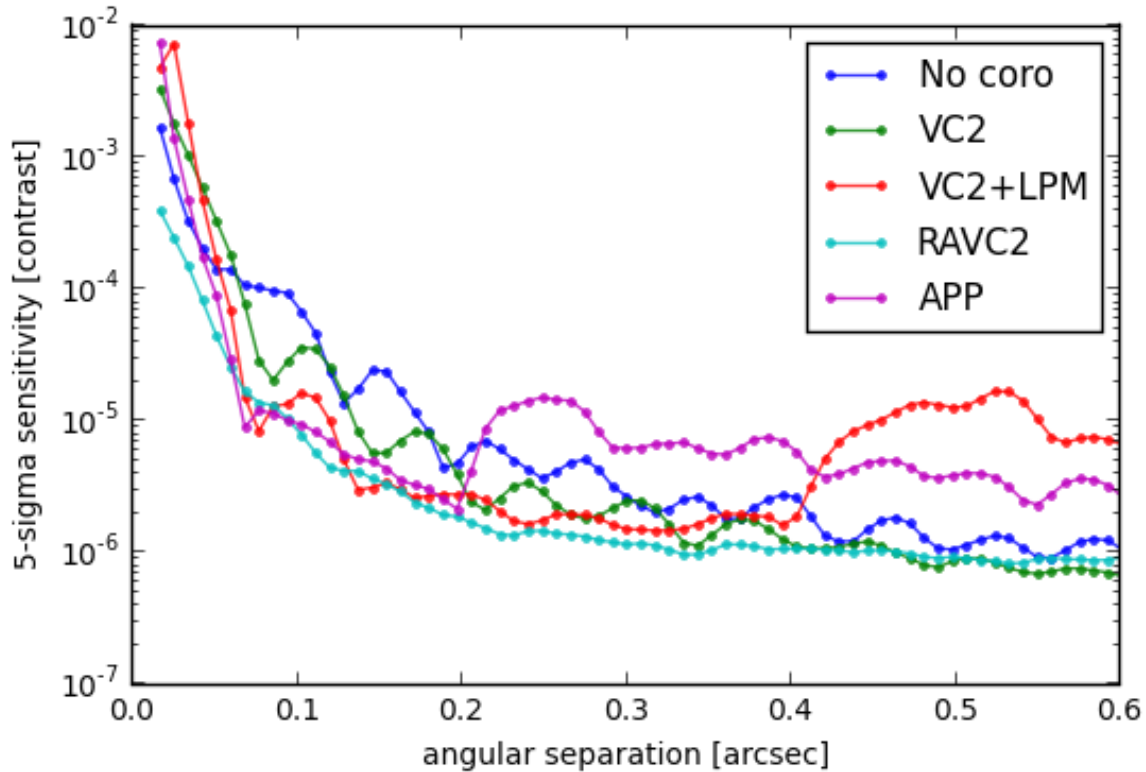


Figure 3. Contrast curves for several different coronagraphs simulated for METIS.

#### 4.1 Vector Apodizing Phase Plate Coronagraphs

Pupil plane coronagraphs can deal with complex pupil geometries and be designed around the secondary support structures and central obscurations of the telescope. The vector Apodizing Phase Plate (vAPP) coronagraphs are pupil plane optics that use the orientation of the fast axis in a liquid crystal polymer to introduce an (achromatic) geometric phase pattern onto the wavefront.<sup>4</sup> They overcome the earlier limitations of the exoplanet discovering<sup>5</sup> APP coronagraphs<sup>6,7</sup> which used variations in the thickness of a Zinc Selenide substrate, and so were chromatic and limited in the phase designs that could be manufactured. The vAPP has three layers of liquid crystal that provide coronagraphic suppression over both L and M bands (Otten et al., ApJ, submitted). This has been demonstrated on-sky at the Magellan AO system with Clio2.

The vAPP coronagraphs can be located either at PP1, or individually in PP3 for the IMG and LMS observing modes (see Figure 4 for a pictorial representation of these modes). The vAPP coronagraphs produce 3 PSFs in the image plane of the IMG mode. Two of the PSFs contain a dark 180 degree wide hole with diffraction suppression from  $2 - 7\lambda/D$ , which when combined provide 360 degrees of coverage. The encircled energy throughput of each pattern is 50%, and splitting the light between the two PSFs reduces this further to 25% total efficiency. A third PSF sits midway between the two coronagraphic PSFs and is referred to as the “leakage term PSF”. This PSF can act as a photometric and astrometric reference for any detected point sources.

#### 4.2 Vortex Coronagraphs

The VC-LPM consists of a focal plane optic called an Annular Groove Phase Mask (AGPM)<sup>8,9</sup> that scatters on-axis light from a star into a subsequent pupil plane that contains a mask that blocks it, while allowing off-axis point sources to be transmitted through to the final focal plane. AGPMs are diamond optics etched via a spallation process to produce a series of annular concentric rings at a sub-wavelength spacing.<sup>10</sup> The optics are  $300\mu\text{m}$  thick with an etched diameter of 10mm, and are anti-reflection coated, optimised for the central wavelength of the band. Early designs of Vortex Coronagraphs used a binary mask for the pupil stop, but

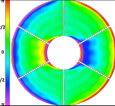
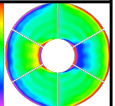
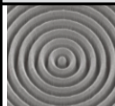
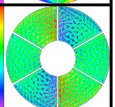
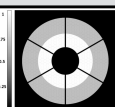
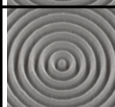


Name of mode	HCI for...	PP1	FP1	FP2	PP3
<b>APP-ALL</b>	<b>IMG/LMS/LongSlit</b>				
<b>APP</b>	<b>IMG/LMS</b>				
<b>VC-LPM</b>	<b>IMG/LMS</b>				
<b>RAVC2</b>	<b>IMG/LMS</b>				
<b>SAM</b>	<b>IMG/LMS</b>				

Figure 4. Table of HCI modes and the location of masks and coronagraphs in the METIS optical path.

simulations show that a Lyot Phase Mask (LPM) provides significantly better rejection with large secondary central obscurations and inner working angle performance. The LPM can also be manufactured using the liquid crystal method described earlier.

An alternative VC design is called a Ring Apodized Vortex Coronagraph (RAVC).<sup>11</sup> This VC design uses a third optic in a pupil plane above the AGPM to optimise the VC performance when there is a large secondary obscuration. The apodizer is an amplitude only gray apodizer, which is circularly symmetric, and can be placed at PP1. This gray apodizer does not need to be derotated with the telescope pupil as it is circularly symmetric, and the reduction in flux does not impact the function of the WFS camera, as the science targets will naturally be very bright and provide significant flux for high signal to noise wavefront sensing.

### 4.3 Sparse Aperture Masks (SAM)

Sparse Aperture Masks (SAMs) mask out the telescope pupil plane to leave a set of apertures whose pairwise combinations form a non-redundant set of baselines, each pair producing a uniquely identifiable set of Young's fringes in the focal plane.<sup>12,13</sup> These fringes can be inverted to reconstruct faint structures at an angular resolution of  $\lambda/2D$ . Currently there is no design for the METIS pupil at this time, but we envisage 2 masks per waveband.

### 4.4 Coronagraphy supported long slit spectroscopy

The CFO and long slit configuration for the LM and NQ cameras cannot support coronagraphic imaging onto the slits at FP2 as the pupil position at PP3 is occupied with a grism for the dispersion. The lack of an available focal plane and pupil plane before FP2 means that no focal plane coronagraph can be implemented for long slit spectroscopy. FP1 is not suitable for a focal plane mask as the wavefront will not be usable for the wavefront sensor camera below it.

The science case for METIS requires high contrast for the long slit spectroscopic mode, and one proposed solution is to manufacture a vAPP optic that has a bandpass capability built into it. This type of bandpass behaviour is possible using liquid crystal deposition technology as demonstrated on CRRES+.<sup>14</sup> Light shorter than 2.8 microns is sent to the WFS unaberrated but the APP phase pattern is encoded in light with wavelengths longer than 2.9 microns to cover the L and M bands. This then acts like a classical APP for slit imaging, but the

APP will have the telescope pupil rotating on it, and so will not be designed around the locations of secondary support structures.

## 5. FOCAL PLANE WAVEFRONT SENSING

The METIS Single Conjugate Adaptive Optics (SCAO) system uses a Shack-Hartmann wavefront sensor (WFS) camera with 74 by 74 subapertures running at 1kHz,<sup>15</sup> forming a closed loop with the actuators within M4. Wavefront aberrations from the atmosphere and telescope optics through the CFO (including the cold stop and derotator) are sensed by the WFS and are corrected. Time-varying aberrations due to thermal variation and flexure of the METIS optics below the location of the AO pickoff dichroic are not sensed or corrected for by this AO loop. These non-common path aberrations (NCPA) produce variations in the diffraction halo of bright stars in the science camera focal plane, which appear as “speckles” with a characteristic size of  $\sim \lambda/D$  when PSF estimation and subtraction is carried out in the data reduction process. Focal plane wavefront sensing (FPWFS) refers to algorithms and methods that can determine the complex amplitude in the pupil plane of the NCPA, and which can subsequently be used during post processing for PSF reconstruction, or if the calculations are fast enough, as an active correction at a rate of 0.1 Hz or so. The focal plane camera records intensity only, with the phase component of the complex electric field lost in the photoelectric conversion process. This results in a degeneracy for the even functioned phase screens in the pupil, and so a known phase diversity must be introduced to provide a mechanism for lifting this degeneracy. We list the possible FPWFS techniques that we are investigating for HCI:

- Phase Sorting Interferometry (PSI) - The AO systems of large telescope provide a well-corrected wavefront that is sensed by the WFS camera. The uncorrected atmospheric aberrations provide enough phase diversity to solve for the complex amplitude in the focal plane of the science camera,<sup>16</sup> and a similar implementation would work with METIS and the E-ELT.
- ZELDA - A phase plate inserted into the focal plane of a camera provides images in the final focal plane that allow for the solving of certain spatial scales of phase.<sup>17</sup> The optic is inserted between science exposures.
- Speckle nulling<sup>18,19</sup> - Using mirror induced probes to supply diversity and then null out the speckles, it has been demonstrated on Keck/NIRC2 and Palomar.
- The COFFEE<sup>20,21</sup> algorithm - Using satellite spots generated by the DM and use them as probes to measure the diversity.
- cMWS - the Coronagraphic Modal Wavefront Sensor (Wilby et al. A&A, submitted) uses a holographic pattern superimposed on a vAPP coronagraph to generate surrounding PSFs that encode the NCPAs within the coronagraphic dark region, enabling simultaneous science and WFS measuring images.

## 6. OBSERVING STRATEGIES

### 6.1 Pupil plane optics

For the vAPP and SAM masks, the observing strategies are simple - they duplicate the non-coronagraphic direct imaging observing modes that include beamswitching for full duty cycles on the acquisition of science data. Dither patterns of 2 or 4 positions on the IMG detectors will produce coronagraphic data for subsequent analysis. The derotator is switched on so that the telescope pupil is fixed with respect to the vAPP optic, enabling complete diffraction suppression accommodating the secondary support structures. This pupil tracking mode is crucial for SAM operations, as any obscuration of the SAM subapertures during an observing block will result in incorrect calibration.

For the LMS, the bright central Airy core of the vAPP presents a challenge for scattered light in the LMS unit past the image slicer. This solution is to move the star so that the bright side and central core of the vAPP PSF (see Figure 5) is moved off one edge of the image slicer, with the dark hole on the slicer. The star is then moved up and down the edge of the slicer, providing beamswitched data in the LMS.

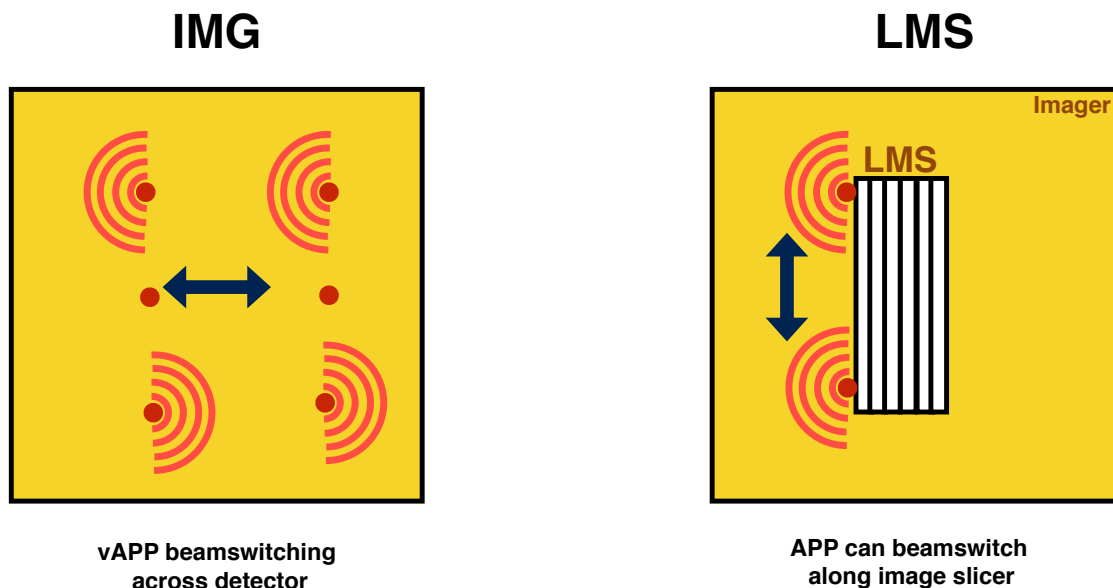


Figure 5. Operational modes for the vAPP and APP coronagraphs on the IMG and LMS modes.

The LongSlit mode uses a vAPP in PP1 which does not have a rotation mechanism for it, and so the secondary support structures are not compensated for in the diffraction suppression. The derotator is engaged so that there are a minimum of rotating surfaces in the optical path.

## 6.2 Vortex Coronagraph Observing

The VC operations will follow the standard operating scheme already developed and validated on sky at Keck/NIRC2, VLT/NACO and LBT/LMIRCam. The differential atmospheric refraction between the WFS wavelengths and the science camera wavelengths cause the star to move off the focal plane coronagraph in a systematic way. A residual circle of light that the secondary obscuration produces in the science camera focal plane provides a method for active optical control of the METIS chopper and a feedback loop to ensure that the star is centered on the VC. The alignment of the star with the vortex center will be aided by the QACITS algorithm,<sup>22</sup> which computes a centering error signal based on the images from the science camera. Once the alignment is performed, this algorithm is run in closed loop to ensure optimal centering during the whole observing sequence, with an accuracy down to  $0.02\lambda/D$  (Huby et al., in prep). The VC observations will generally take advantage of Angular Differential Imaging,<sup>23</sup> where the derotator tracks the pupil, and the field rotates on the detector. We anticipate that, for exoplanet imaging, typical ADI sequences of about an hour will be performed around transit at meridian. Based on preliminary ADI contrast curves,<sup>3</sup> we expect to reach a contrast down to 15 mag at a fraction of an arcsecond from bright stars.

Atmospheric dispersion disperses the stellar image into a spectrum along the great circle between the zenith and the science target. There is no atmospheric dispersion corrector in the METIS science camera beam, and so these small spectra limit the suppression factor of the VC. Simulations show that these are negligible for the M and N bands, and only become significant for the wide L band filter if the zenith distance is greater than 45 degrees, which is not expected to be a typical observing setup for HCI.

## 7. CONCLUSION

We have presented the high contrast imaging modes for the METIS baseline design in all observing modes, along with proposals for the compensation of residual speckles in the dark haloes of the coronagraphs. Remaining issues include the testing of the RAVC design, full AO simulations that include the effect of telescope vibrations that



can affect focal plane coronagraph performance, and the TRL of the bandpass vAPP for the LongSlit observing mode.

## REFERENCES

- [1] McPherson, A., Spyromilio, J., Kissler-Patig, M., Ramsay, S., Brunetto, E., Dierickx, P., and Cassali, M., “E-elt update of project and effect of change to 39m design,” *Proc. SPIE* **8444**, 84441F–84441F–9 (2012).
- [2] Agocs, T., “Preliminary optical design for the common fore optics of METIS,” in [*Ground-based and Airborne Instrumentation for Astronomy VI*], *SPIE* **9908** (Aug. 2016).
- [3] Carlomagno, B., Absil, O., Kenworthy, M. and Ruane, G., U., K. C., Otten, G., Feldt, M., Hippler, S., Huby, E., Mawet, D., Delacroix, C., Surdej, J., Habraken, S., Forsberg, P., Karlsson, M., and Catalan, E. B., “End-to-end simulations of the E-ELT/METIS coronagraphs,” in [*Adaptive Optics Systems V*], *SPIE* **9909** (Aug. 2016).
- [4] Snik, F., Otten, G., Kenworthy, M., Miskiewicz, M., Escuti, M., Packham, C., and Codona, J., “The vector-APP: a broadband apodizing phase plate that yields complementary PSFs,” in [*Society of Photo-Optical Instrumentation Engineers (SPIE) Conference Series*], *Society of Photo-Optical Instrumentation Engineers (SPIE) Conference Series* **8450** (Sept. 2012).
- [5] Quanz, S. P., Amara, A., Meyer, M. R., Kenworthy, M. A., Kasper, M., and Girard, J. H., “A Young Protoplanet Candidate Embedded in the Circumstellar Disk of HD 100546,” *ApJL* **766**, L1 (Mar. 2013).
- [6] Codona, J. L. and Angel, R., “Imaging Extrasolar Planets by Stellar Halo Suppression in Separately Corrected Color Bands,” *ApJL* **604**, L117–L120 (Apr. 2004).
- [7] Kenworthy, M. A., Codona, J. L., Hinz, P. M., Angel, J. R. P., Heinze, A., and Sivanandam, S., “First On-Sky High-Contrast Imaging with an Apodizing Phase Plate,” *ApJ* **660**, 762–769 (May 2007).
- [8] Mawet, D., Riaud, P., Surdej, J., and Baudrand, J., “Subwavelength surface-relief gratings for stellar coronagraphy,” *Applied Optics* **44**, 7313–7321 (Dec. 2005).
- [9] Mawet, D., Riaud, P., Absil, O., and Surdej, J., “Annular Groove Phase Mask Coronagraph,” *ApJ* **633**, 1191–1200 (Nov. 2005).
- [10] Delacroix, C., Forsberg, P., Karlsson, M., Mawet, D., Absil, O., Hanot, C., Surdej, J., and Habraken, S., “Design, manufacturing, and performance analysis of mid-infrared achromatic half-wave plates with diamond subwavelength gratings,” *Appl. Opt.* **51**, 5897–5902 (Aug 2012).
- [11] Mawet, D., Pueyo, L., Carlotti, A., Mennesson, B., Serabyn, E., and Wallace, J. K., “Ring-apodized Vortex Coronagraphs for Obscured Telescopes. I. Transmissive Ring Apodizers,” *ApJS* **209**, 7 (Nov. 2013).
- [12] Tuthill, P., Lloyd, J., Ireland, M., Martinache, F., Monnier, J., Woodruff, H., ten Brummelaar, T., Turner, N., and Townes, C., “Sparse-aperture adaptive optics,” in [*Society of Photo-Optical Instrumentation Engineers (SPIE) Conference Series*], *Society of Photo-Optical Instrumentation Engineers (SPIE) Conference Series* **6272** (July 2006).
- [13] Lloyd, J. P., Martinache, F., Ireland, M. J., Monnier, J. D., Pravdo, S. H., Shaklan, S. B., and Tuthill, P. G., “Direct Detection of the Brown Dwarf GJ 802B with Adaptive Optics Masking Interferometry,” *ApJL* **650**, L131–L134 (Oct. 2006).
- [14] Hornburg, K. J., Komanduri, R. K., and Escuti, M. J., “Multiband retardation control using multi-twist retarders,” *Proc. SPIE* **9099**, 90990Z–90990Z–9 (2014).
- [15] Stuik, R., “Designing the METIS SCAO and LTAO systems,” in [*Adaptive Optics Systems V*], *SPIE* **9909** (Aug. 2016).
- [16] Codona, J. L. and Kenworthy, M., “Focal Plane Wavefront Sensing Using Residual Adaptive Optics Speckles,” *ApJ* **767**, 100 (Apr. 2013).
- [17] N’Diaye, M., Vigan, A., Dohlen, K., Sauvage, J.-F., Caillat, A., Costille, A., Girard, J. H. V., Beuzit, J.-L., Fusco, T., Blanchard, P., Le Merrer, J., Le Mignant, D., Madec, F., Moreaux, G., Mouillet, D., Puget, P., and Zins, G., “Calibration of quasi-static aberrations in exoplanet direct-imaging instruments with a Zernike phase-mask sensor. II. Concept validation with ZELDA on VLT/SPHERE,” *ArXiv e-prints* (June 2016).
- [18] Bottom, M., “Speckle nulling wavefront control for Palomar and Keck,” in [*Adaptive Optics Systems V*], *SPIE* **9909** (Aug. 2016).

- [19] Martinache, F., Guyon, O., Jovanovic, N., Clergeon, C., Singh, G., Kudo, T., Currie, T., Thalmann, C., McElwain, M., and Tamura, M., “On-Sky Speckle Nulling Demonstration at Small Angular Separation with SCE<sub>x</sub>AO,” *PASP* **126**, 565–572 (June 2014).
- [20] Mugnier, L. M., “High spatial frequency diversity for coronagraphic wavefront sensing with COFFEE,” in [*Space Telescopes and Instrumentation 2016: Optical, Infrared, and Millimeter Wave*], *SPIE* **9904** (Aug. 2016).
- [21] Paul, B., Sauvage, J.-F., and Mugnier, L. M., “Coronagraphic phase diversity: performance study and laboratory demonstration,” *A&A* **552**, A48 (Apr. 2013).
- [22] Huby, E., Baudoz, P., Mawet, D., and Absil, O., “Post-coronagraphic tip-tilt sensing for vortex phase masks: The QACITS technique,” *A&A* **584**, A74 (Dec. 2015).
- [23] Marois, C., Lafrenière, D., Doyon, R., Macintosh, B., and Nadeau, D., “Angular Differential Imaging: A Powerful High-Contrast Imaging Technique,” *ApJ* **641**, 556–564 (Apr. 2006).